Materials Research Proceedings 28 (2023) 1047-1056 https://doi.org/10.21741/9781644902479-115

Flange wrinkling in incremental shape rolling

ESSA Abdelrahman[1,a] *, ABEYRATHNA Buddhika[1,b], ROLFE Bernard[2,c], and WEISS Matthias[1,d]

[1]Institute for Frontier Materials, Deakin University, Waurn Ponds, Pigdons Rd., Geelong, VIC 3216, Australia

[2]School of Mechanical Engineering, Deakin University, Waurn Ponds, Pigdons Rd., Geelong, VIC 3216, Australia

[a]aessa@deakin.edu.au, [b]buddhika.abeyrathna@deakin.edu.au, [c]bernard.rolfe@deakin.edu.au, [d]matthias.weiss@deakin.edu.au

Keywords: Incremental Shape Rolling, Flexible Roll Forming, Finite Element Analysis, Wrinkling

Abstract. Automotive structural components from Advanced High Strength Steels (AHSS) can be manufactured with Flexible Roll Forming (FRF). Flange wrinkling is a common shape defect in FRF, this restricts the application of FRF in the automotive industry. The new Incremental Shape Rolling process (ISR) showed that a high tensile transverse strain is developed in the flange and that assists the plastic deformation in the flange. Hence, wrinkle severity can be significantly reduced when weight-optimized components are formed. In this study, the ISR process is applied to a variable width profile from DP600. This investigated profile is a modified automotive component. The forming strains and wrinkling severity in ISR are compared with those obtained from the FRF case. The ISR and the FRF experimental trials are performed on a prototype FRF facility and then used to validate the numerical models which are applied to analyse the deformation behaviour in both processes. The ISR results show a significant reduction in wrinkling. This is due to the high tensile transverse strain that is developed in the ISR flange which facilitates the plastic deformation and hence the flange is stably compressed to the required shape.

Nomenclatures

d_y	Increment size
f	Flange length
MAE	Mean absolute error
n	Number of points considered for the wrinkling evaluation
R	Radius of the pre-cut blank
R_n	Roll nose radius
r_i	Inner radius of the part
t	Material thickness
XYZ	Global coordinate system
xyz	Local coordinate system
xi	X coordinate of the deformed flange edge
$\hat{x}_i$	X coordinate of the ideal flange edge
ε_{th}	Theoretical required longitudinal strain
φ	Bend angle

Materials Research Proceedings 28 (2023) 1047-1056 https://doi.org/10.21741/9781644902479-115

Introduction

Advanced High Strength Steels AHSS are increasingly used in the automotive industry for structural components due to their high strength-to-weight ratio [1, 2]. Roll Forming (RF) is a common forming process for the manufacturing of lightweight automotive structural components from high-strength and low-ductility materials [3]. However, RF is limited to the forming of simple components that have a constant cross-section [4]. Flexible roll forming was therefore developed to enable the forming of complex components with cross-sections that vary along the length of the profile [5]. Flange wrinkling is one of the common shape defects in FRF [6] and occurs if the required longitudinal compressive strain in the flange cannot be achieved by stable compression [7]. Limited practical solutions have been proposed to eliminate flange wrinkling, this restricts the shape complexity achievable with FRF from AHSS [6, 8].

Recently, a prototype flexible roll forming facility has been introduced [9, 10] and special forming tooling developed that supports the flange during the deformation and reduces flange wrinkling. However, wrinkling is still observed when flexible roll forming high-strength sheet metal [9] and this limits the widespread application of FRF in the automotive industry.

Incremental Sheet Forming (ISF) processes such as metal spinning and single-or-two point incremental forming are characterized by localized deformation which improves the formability and shape quality [11]. The axial tensile deformation that is formed during the forward paths in metal spinning balances the compressive hoop stress and this allows the forming of wrinkle-free spun [12, 13]. However, due to the limited working range of the ISF milling machines, forming long automotive structural sections is not feasible [14]. In addition, ISF of high-strength materials needs warm forming techniques to reduce the material strength [15].

The new Incremental Shape Rolling process has been recently developed and applied for the forming of long and straight U-profile components [16]. Similar to ISF, a high transverse tensile strain is developed in the flange and this promises to facilitate the plastic deformation in the flange when ISR is applied to weight-optimized components from AHSS.

In this study, the new ISR process is applied to manufacture the critical region of a simplified automotive component with a changing width cross-section. The same component shape is formed with the conventional FRF process on the same prototype forming facility [9] and the material deformation and shape defects are compared between both processes. Abaqus implicit is then used to further analyse the deformation behaviour in both processes.

Profile Geometry and Material

The investigated component has a cross-section that varies in width along its length, see Fig. 1a. The component has a flange length of f = 18 mm, an inner radius r_i = 5 mm and a material thickness of t =1.5 mm. Wrinkling is only expected to occur in the compression side of the component, where the flange is longitudinally compressed. On the other side, the flange is longitudinally stretched. Therefore, only the compression side of the component is considered in this study and due to shape symmetry around the X-Y plane, only one-quarter of the component is investigated (the highlighted quarter). The pre-cut blank corresponding to the investigated quarter of the component is shown in Fig. 1b. Standard tensile tests were carried out on an Instron 5967 with a 30 kN load cell according to ASTM E8/E8M [17]. The tensile tests were done along the rolling direction and at a test speed of 0.025 mm s^{-1}. The averaged true stress–true strain curve of the DP600 sheet is shown in Fig. 1c. The mechanical properties are obtained by fitting the Hollomon's power law of the tested material and are shown in Table 1.

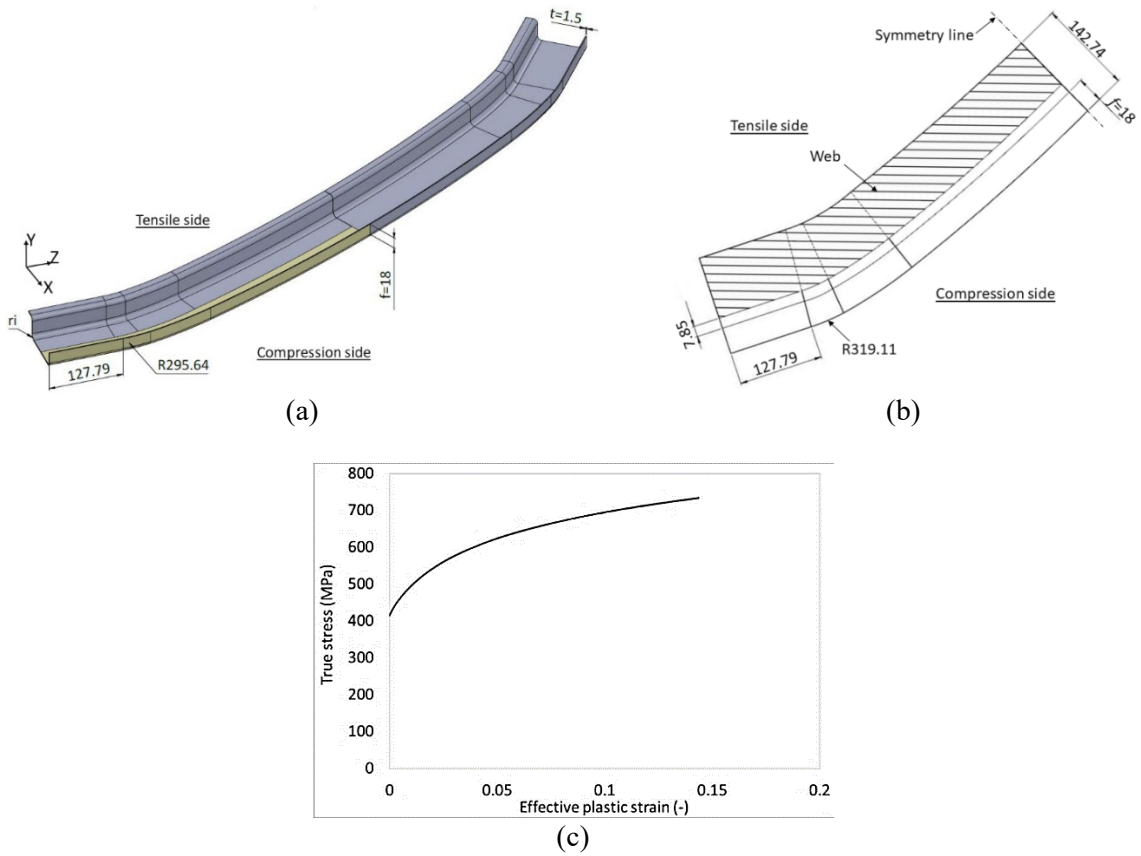

Fig. 1. Schematic showing (a) the full variable width profile and (b) the pre-cut blank corresponding to the investigated quarter of the component and (c) the average true stress-effective plastic strain curve of the DP600 sheet (dimensions in mm).

Table 1. Tensile data of the DP600 sheet.

Material	Thickness t (mm)	0.2% Yield strength (MPa)	Ultimate tensile strength (MPa)	Strain hardening	Strength coefficient (MPa)
DP600	1.5	414.5	733.5	0.11	897

Experimental Trials

Incremental Shape Rolling.

In ISR, the pre-cut blank is held between the clamping dies with the force applied by six hydraulic cylinders. A cylindrical forming roll with a roll nose radius, R_n=1 mm was used, see Fig. 2, and an initial clearance between the forming roll and the top die set to the sheet thickness, *t*. The hexapod which carries the forming roll has six degrees of freedom. During forming the roll is first moved up incrementally in Y-direction, d_y, and then moved in the X-Z plane to follow the top die contour while keeping the initial clearance, *t*. The roll rotates around the Y-axis to keep its axis perpendicular to the roll path. At the same time, the clamping dies move linearly in the longitudinal Z-direction. This roll path is repeated several times until the blank is fully formed over the top die.

Materials Research Proceedings 28 (2023) 1047-1056 https://doi.org/10.21741/9781644902479-115

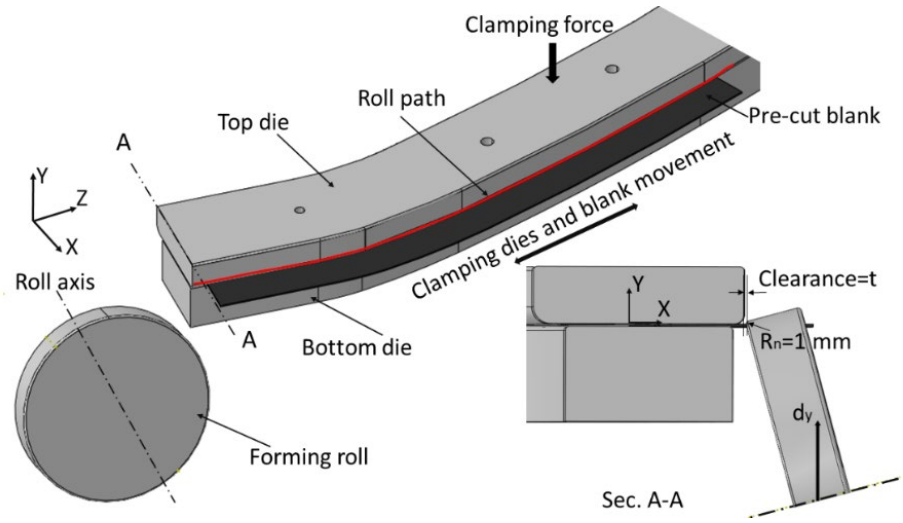

Fig. 2. Schematic drawing of the ISR process of the variable width profile.

The same ISR forming sequence as applied for the ISR of straight components in previous work [16] was implemented in this investigation, where the flange incrementally wraps over the roll nose radius in each pass, and in this way, the flange is formed upwards until the pre-cut is fully formed to the desired shape. In this study, the smallest possible increment size d_y=1 mm was used, as it is reported that the transverse tensile strain increases with decreasing the increment size, d_y [16] which provides the best possible flange quality.

Flexible Roll Forming.

The flexible roll forming trials were done on Deakin's FRF facility, where the blank is held between the clamping dies by six-hydraulic cylinders. One bottom roll (B1) is used to incrementally bend the pre-cut blank into shape with 14 forming passes. This represents the simplest forming and tool approach. More complex forming tools using finger rolls have been applied in previous studies to significantly reduce wrinkling and improve part shape [18]. In this study, a higher winkling tendency was desired to provide a clear difference in forming modes between the ISR and the FRF approach. The corresponding bend angle increment in FRF is 11°, 7°, 10°, 5°, 8°, 5°, 6°, 6°, 6°, 6°, 5°, 5°, 5°, 5°. The left side of Fig. 3 shows the schematic of the relative contact between the roll and the flange during forming, while the FRF bend sequence is shown on the right side of Fig. 3.

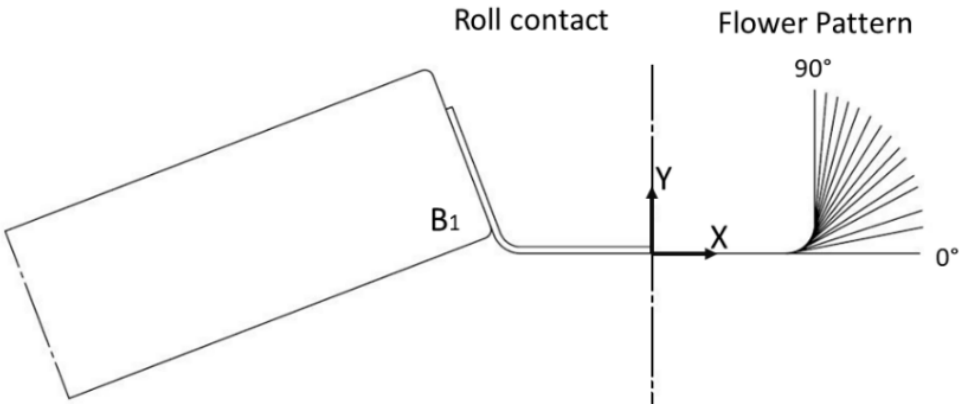

Fig. 3. Schematic of the roll set used in the FRF process and the implemented flower pattern.

Shape Analysis and Strain Measurement.
A 3D laser scanner "CreaForm HandyScan 700" [19] has been used to scan the flange after the final forming pass and before the part was released from the clamping dies. The data was then imported into the Geomagic Qualify software [20] to evaluate the flange quality and to compare it to the ideal shape of the flange. For this, a X-Z plane section cut was created along the length of the flange and located at a distance of 1 mm under the flange edge, see Fig. 4.

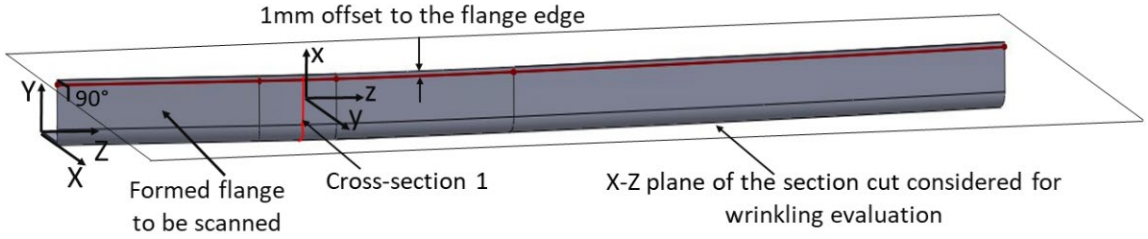

Fig. 4. Formed flange and the path considered for wrinkling evaluation.

Eq. 1 was used to calculate the mean absolute error (MAE) of the flange edge [9] to quantitatively evaluate flange wrinkling. The wrinkles were observed at a *Z*-coordinate of 70 to 320 mm measured from the lead end of the component and the MAE was therefore calculated in this region, see Fig. 5. Note that, the lead end is the component end where the forming pass starts while the tail end is where the forming pass ends.

$$MAE = \frac{1}{n} \sum_{i=1}^{n} |x_i - \hat{x}_i|. \quad (1)$$

Where, $\hat{x}_i$ is the corresponding *X* coordinate of the ideal flange edge, *xi* is the *X* coordinate of the deformed flange edge and *n* is the number of points considered for the wrinkling evaluation.

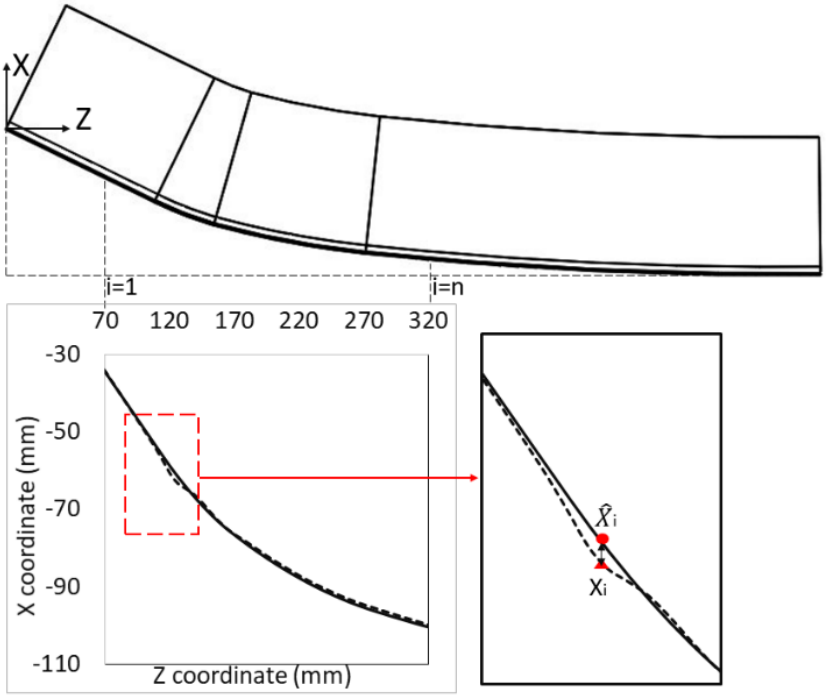

Fig. 5. Flange edge considered for the wrinkling analysis.

The AutoGrid strain measuring system [21] was used to measure the true major and minor strains after the final forming pass and after the component had been removed from the clamping dies. For this, a 2 mm × 2 mm grid was printed on the pre-cut blank and pictures of the formed grid were taken with a camera. The strain components were evaluated in cross-section 1 (S1) in the middle of the critical radius, R=295.64 mm (see Fig. 1a and 6). The local coordinate system (xyz) which follows the formed material was used to plot the strain components; where PExx is the transverse strain and PEzz is the longitudinal strain, while (XYZ) is the global coordinate system, see Fig. 4.

Eq. 2 was used to calculate the theoretical longitudinal strain, ε_{th}, required to form the flange. The R319.11 mm is the most critical radius in the compression side of the pre-cut blank (see Fig. 1a) and this results in the highest longitudinal compression strain in the flange, and severe wrinkling is expected to occur in this critical radius [9]. Based on Eq. 2 the theoretical longitudinal strain that is needed to form the flange in this critical radius is ε_{th} = -0.054.

$$\varepsilon_{th} = ln\frac{R - f(1-cos\varphi)}{R}. \quad (2)$$

Where ε_{th} is the theoretical required longitudinal strain, R is the radius of the pre-cut blank, f is the flange length and φ is the required bend angle of 90°.

Finite Element Analysis

The finite element simulation of the ISR process and FRF process have been performed with Abaqus Implicit. The clamping dies and the forming roll were modelled as rigid bodies, while the pre-cut blank has been discretized with reduced integration, hexahedral, linear brick elements (C3D8R). Four elements through the blank thickness were used with an element size of 1 mm and 2.5 mm in the X and the Z directions, respectively. A "frictionless contact" was assumed between the forming roll and the blank surfaces to avoid convergence issues [22]. To minimize the penetration of the rigid bodies into the blank surfaces at the constraint locations, the "hard contact condition" was applied [23]. The true stress-effective plastic strain curve shown in Fig. 1c was used together with isotropic hardening and the von Mises yield criteria to define the plastic material behaviour of the DP600 sheet [24, 25]. The elastic properties were defined with Poisson's ratio, ν, which is assumed to be 0.3 [9] and a Young's modulus of 200 GPa [26]. For the analysis of the forming results, the same procedure as used in the experimental trials is applied.

Results

Evaluation of Flange Wrinkling.

Fig. 6a compares the formed flange shape with the ideal shape of the flange after the final forming pass for both FRF and ISR. For a clear presentation, a 10 mm X-offset is applied between each forming case. The experimental results show that a clear wrinkle is formed in the FRF flange while the final shape of the ISR flange is close to the ideal shape. The FEA results underestimate the shape error and only indicate the formation of a buckle in the FRF flange, while there is no wrinkling predicted for the ISR process which correlates with the experimental results. Fig. 6b shows the calculated MAE for each forming case. The FEA results of the MAE accurately predict the experimental trend.

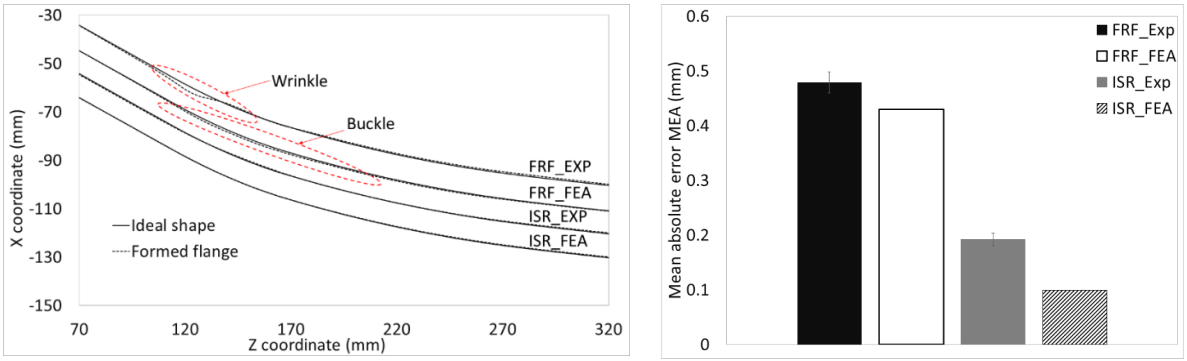

(a) (b)

Fig. 6. (a) Comparison of the flange edge shape after the final forming pass and (b) MAE of the flange edge.

Material Deformation in the Flange.

The distribution of the transverse and the longitudinal residual strain along Section 1, i.e., in the middle length of the critical radius (see Fig. 4) was measured after the final forming pass and is given in Fig. 7a and b, respectively. The Autogrid system gives a good measurement along the flange length, while a strain measurement was not possible in the profile radius area zone, r_i. The experimental results and the FEA results suggest that a high transverse and longitudinal strain develops in the ISR flange, while there is only a very small level of transverse tensile strain and longitudinal strain in the FRF flange, see Fig. 7. The longitudinal compressive strain that is formed in the ISR flange reaches the theoretically required longitudinal, ε_{th}, in the flange edge, see Fig. 7b. In contrast, the longitudinal compressive strain that develops in the FRF flange is significantly lower than the theoretically required strain, ε_{th}.

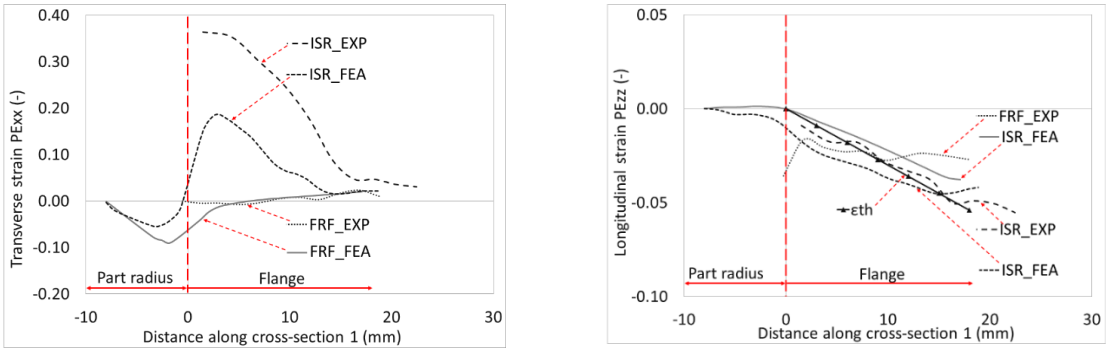

(a) (b)

Fig. 7. Residual strain along cross-section 1 after the final forming pass (a) transverse direction and (b) longitudinal direction.

Discussion

The Effect of the Forming Method on Wrinkling Severity.

In ISR, the flange is wrapped over the roll nose radius to a larger extent in the early forming passes compared to that in the later forming passes [16]. Thus, the formed transverse tensile strain in ISR reaches its maximum level above the part radius, r_i, and then drops back to reach a minimum at the flange edge, see Fig. 7a.

To produce a complex part contour without wrinkling, the flange needs to compress longitudinally [7]. Eq. 2 was used to calculate the theoretical longitudinal strain, ε_{th}, required in

the flange to produce the investigated component. As can be seen in Fig. 7a, ISR results in a high tensile transverse strain. This high transverse strain assists in forming the longitudinal compressive strain that is required to form the investigated flange. As shown in Fig. 7b, the formed longitudinal compressive strain in the flange reaches the theoretically required longitudinal strain. This indicates that the material is stably compressed in the critical zone without wrinkling.

In FRF, bending is the major deformation mechanism in the transverse direction and therefore the transverse tensile strain is low. This results in a small compressive longitudinal strain that is lower than that theoretically required. This means that in FRF the edge length remains longer than required and that therefore the compressive longitudinal stress is released in form of wrinkling rather than stable compression. This explains the severe flange wrinkling that occurred when FRF the component with the simple tooling, see Fig. 6a.

Both the experimental result and the FEA result of the FRF case suggest the formation of a buckle after pass 5, which forms into a wrinkle after pass 7 in the experimental trials. The longitudinal membrane stress, S_{zz}, is investigated along the selected node path in the flange edge (see Fig. 8a) for both the FRF (Fig. 8b) and the ISR case (Fig. 8c). For both processes, the maximum longitudinal compressive stress occurred in the critical radius, R295.64, see Fig. 1a. In FRF, the longitudinal compressive stress increases with the forming passes and reaches the critical buckling initiation stress of 527 MPa [9] after pass 5 (Fig. 8b), which is where the initial buckle was observed. Note that as soon as the buckle initiates the stress will release, i.e., there will be no further stress increase. The residual longitudinal stress formed in ISR is lower than the critical buckling stress and decreases with the forming passes (Fig. 8c). This suggests that the transverse tensile stress that is generated in the flange reduces the longitudinal compressive stress and therefore prevents the development of a wrinkle.

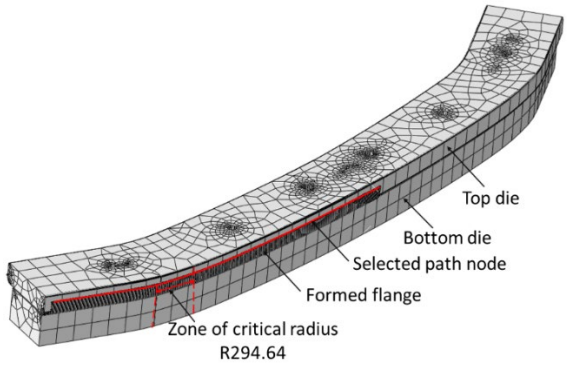

(a)

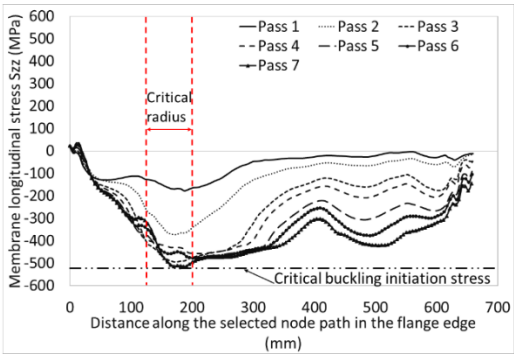

(b)

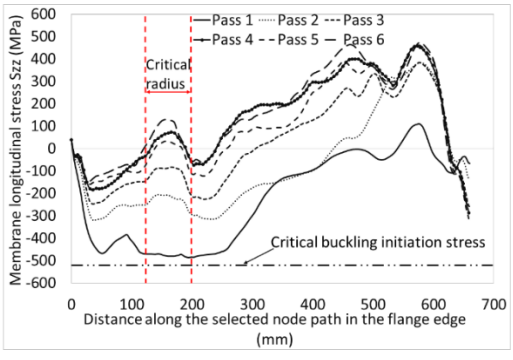

(c)

Fig. 8. (a) Node path considered for analysis of longitudinal stress, (b) evaluation of membrane longitudinal stress at the selected node path for FRF and (c) for ISR.

Summary

In this study, the incremental shape rolling of an automotive component with variable width was investigated and the deformation mechanisms and shape quality compared with those obtained from FRF. The major outcomes of this study are:

- ISR enables the manufacture of weight-optimized automotive components from high-strength steel by eliminating the wrinkling severity.
- In ISR, the transverse tensile strain results from the material wrapping over the roll radius.
- The transverse tensile strain that is developed in the ISR flange assists in the forming of the longitudinal compressive strain that is required to form the part contour. In FRF, the transverse and longitudinal strains are low. This leads to wrinkling instead of stable longitudinal compression in the flange.
- ISR represents a promising alternative to conventional sheet forming processes where excessive wrinkling leads to issues.

Acknowledgements

The authors acknowledge data M Sheet Metal Solutions GmbH for the development and manufacture of the 3D roll forming prototyping facility. The authors would like to thank Deakin University Postgraduate Research Scholarships (DUPRS) for their financial support.

References

[1] N. Baluch, Z.M. Udin, C.S. Abdullah, Advanced high strength steel in auto industry: an overview, Eng. Appl. Sci. Res. 4 (2014) 686-689. https://doi.org/10.48084/etasr.444

[2] G. Sun, M. Deng, G. Zheng, Q. Li, Design for cost performance of crashworthy structures made of high strength steel, Thin-Walled Struct. 138 (2019) 458-472. https://doi.org/10.1016/j.tws.2018.07.014

[3] A.D. Deole, M.R. Barnett, M. Weiss, The numerical prediction of ductile fracture of martensitic steel in roll forming, Int. J. Solids. Struct. 144-145 (2018) 20-31. https://doi.org/10.1016/j.ijsolstr.2018.04.011

[4] C. Jiao-Jiao, C. Jian-Guo, Z. Qiu-Fang, L. Jiang, Y. Ning, Z. Rong-guo, A novel approach to springback control of high-strength steel in cold roll forming, Int. J. Adv. Manuf. Technol. 107 (2020) 1793-1804. https://doi.org/10.1007/s00170-020-05154-8

[5] Y. Yan, H. Wang, Q. Li, B. Qian, K. Mpofu, Simulation and experimental verification of flexible roll forming of steel sheets, Int. J. Adv. Manuf. Technol. 72 (2014) 209-220. https://doi.org/10.1007/s00170-014-5667-0

[6] M.M. Kasaei, H.M. Naeini, G.H. Liaghat, C.M.A. Silva, M.B. Silva, P.A.F. Martins, Revisiting the wrinkling limits in flexible roll forming, J. Strain. Anal. Eng. Des. 50 (2015) 528-541. https://doi.org/10.1177/0309324715590956

[7] M.M. Kasaei, H.M. Naeini, B. Abbaszadeh, M. Mohammadi, M. Ghodsi, M. Kiuchi, R. Zolghadr, G. Liaghat, R.A. Tafti, M. S. Tehrani, Flange wrinkling in flexible roll forming Process, Procedia Eng. 81 (2014) 245-250. https://doi.org/10.1016/j.proeng.2014.09.158

[8] P. Groche, A. Zettler, S. Berner, G. Schneider, Development and verification of a one-step-model for the design of flexible roll formed parts, Int. J. Mater. Form. 4 (2010) 371-377. https://doi.org/10.1007/s12289-010-0998-3

[9] B. Abeyrathna, S. Ghanei, B. Rolfe, R. Taube, M. Weiss, Optimising part quality in the flexible roll forming of an automotive component, Int. J. Adv. Manuf. Technol. 118 (2021) 3361-3373. https://doi.org/10.1007/s00170-021-08176-y

[10] S. Ghanei, B. Abeyrathna, B. Rolfe, M. Weiss. Analysis of material behaviour and shape defect compensation in the flexible roll forming of advanced high strength steel. In: IOP Conf Ser Mater Sci Eng.vol. 651. IOP Conf Ser Mater Sci Eng; 2019. https://doi.org/10.1088/1757-899x/651/1/012064.

[11] S. Gatea, H. Ou, G. McCartney, Review on the influence of process parameters in incremental sheet forming, Int. J. Adv. Manuf. Technol. 87 (2016) 479-499. https://doi.org/10.1007/s00170-016-8426-6
[12] O. Music, J.M. Allwood, K. Kawai, A review of the mechanics of metal spinning, J. Mater. Process. Technol. 210 (2010) 3-23. https://doi.org/10.1016/j.jmatprotec.2009.08.021
[13] Z. Jia, L. Li, Z. R. Han, Z. J. Fan, B. M. Liu, Experimental study on wrinkle suppressing in multi-pass drawing spinning of 304 stainless steel cylinder, Int. J. Adv. Manuf. Technol. 100 (2018) 111-116. https://doi.org/10.1007/s00170-018-2712-4
[14] A.K. Behera, R.A. de Sousa, G. Ingarao, V. Oleksik, Single point incremental forming: An assessment of the progress and technology trends from 2005 to 2015, J. Manuf. Process. 27 (2017) 37-62. https://doi.org/10.1016/j.jmapro.2017.03.014
[15] A. Kumar, V. Gulati, P. Kumar, H. Singh, Forming force in incremental sheet forming: a comparative analysis of the state of the art, J. Braz. Soc. Mech. Sci. Eng. 41 (2019). https://doi.org/10.1007/s40430-019-1755-2
[16] A. Essa, B. Abeyrathna, B. Rolfe, M. Weiss, Prototyping of straight section components using incremental shape rolling, Int. J. Adv. Manuf. Tech. 121 (2022) 3883-3901. https://doi.org/10.1007/s00170-022-09600-7
[17] ASTM Standard, Standard Test Methods for Tension Testing of Metallic Materials, in, ASTM International, 2016.
[18] A. Sreenivas, B. Abeyrathna, B. Rolfe, M. Weiss, Longitudinal strain and wrinkling analysis of variable depth flexible roll forming, J. Manuf. Process. 81 (2022) 414-432. https://doi.org/10.1016/j.jmapro.2022.06.063
[19] Information on https://www.creaform3d.com/en;
[20] Information on http://www.geomagic.com/en/;
[21] Information on https://www.vialux.de/en/;
[22] M. Weiss, B. Abeyrathna, D.S. Gangoda, J. Mendiguren, H. Wolfkamp, Bending behaviour and oil canning in roll forming a steel channel, Int. J. Adv. Manuf. Technol. 91 (2017) 2875-2884. https://doi.org/10.1007/s00170-016-9892-6
[23] Y.Y. Woo, S.W. Han, I.Y. Oh, Y.H. Moon, Shape defects in the flexible roll forming of automotive parts, Int J Automot. Technol. 20 (2019) 227-236. https://doi.org/10.1007/s12239-019-0022-y
[24] B. Abeyrathna, B. Rolfe, L. Pan, R. Ge, M. Weiss, Flexible roll forming of an automotive component with variable depth, Adv. Mater. Process. Technol. 2 (2016) 527-538. https://doi.org/10.1080/2374068x.2016.1247234
[25] B. Abeyrathna, B. Rolfe, J. Harrasser, A. Sedlmaier, G. Rui, L. Pan, M. Weiss. Prototyping of automotive components with variable width and depth. In: 36th IDDRG Conference.vol. 36th IDDRG Conference; 2017. https://doi.org/10.1088/1742-6596/896/1/012092
[26] B. Abeyrathna, B. Rolfe, M. Weiss, The effect of process and geometric parameters on longitudinal edge strain and product defects in cold roll forming, Int. J. Adv. Manuf. Technol. 92 (2017) 743-754. https://doi.org/10.1007/s00170-017-0164-x